Research Article

AC EOF in a rectangular microannulus

Ali Jabari Moghadam[1]

Received: 30 September 2019 / Accepted: 26 November 2019 / Published online: 28 November 2019

Abstract
Electrokinetic flow under an alternating current electric field is numerically studied in a rectangular microannulus whose inner and outer surfaces may have different zeta potentials. The main parameters that affect the shape of the flow field are electrokinetic diameter, dimensionless frequency, surface charge ratio, aspect ratio, and hydraulic diameter. An increase in the electrokinetic diameter leads to a decrease in the effective electric double layer thickness, while the reverse is true for the Poiseuille number, maximum velocity near the wall, and the flow rate. Very low-frequency flow exhibits lid-like velocity profiles; on the contrary, very high-frequency flow represents thin oscillating layers close to the walls and a nearly stationary bulk fluid. Within the limit of higher-than-one excitation frequencies, the response of the liquid inside the electric double layer to the time-periodic electric field is almost immediate, while the rest needs a finite time to follow the instantaneous changes in the applied electric field. Instantaneous one- or two-direction flow can be produced, depending on the relative sign of the surface charges. For a fixed value of the electrokinetic diameter, the Poiseuille number increases and the flow rate decreases as a result of an increase in the hydraulic diameter.

Keywords Time-periodic electroosmotic flow · Rectangular annulus · Frequency · Poiseuille number · Flow rate

1 Introduction

Microelectromechanical systems (MEMS) have been developed considerably over recent years. The electronic integrated circuits and MEMS may naturally lead to lab-on-a-chip (LOC) systems which are thought of as the shrinking of an entire laboratory to a chip. Reduction in the amount of required sample and development of compact systems in handling and analyzing some conducting liquids are the advantages of microscale devices. A LOC system is a reasonable combination of microchannels, electrodes, and some other components with the typical channel sizes on the order of several tens of micrometers. If an electrolyte is in contact with a solid wall, it will get oppositely charged while preserving global charge neutrality. A region will then exist where the concentration of counterions is larger than that of the coions. An electric double layer (EDL) is therefore formed close to the wall which has two distinct layers: an immobile stern layer and a mobile diffuse layer. If an external electric field is applied along the microtube, the mobile ions in the diffuse layer will move; the bulk fluid will then be dragged by the viscous action. The main advantage of electroosmosis (rather than pressure-driven means) is to eliminate (or at least, to reduce) the necessity for mechanical pumping especially in micro-scale devices. As microchannels have very large surface area to volume ratio, relatively large values of pressure gradient are needed to make the fluid in motion. Electroosmosis, however, concerns with electric forces on ions in the EDL which is caused by voltage signals sent to electrodes. A plug-like velocity profile is therefore attained in the cross-sectional area which is uniform far from the wall but reduces to zero at the wall over the Debye length on the order of a few nanometers [1–4].

Numerous studies were conducted to explore the behavior of electroosmotic flow (EOF) in micro-scale

✉ Ali Jabari Moghadam, jm.ali.project@gmail.com | [1]Faculty of Mechanical Engineering, Shahrood University of Technology, P.O. Box 316, Shahrood 3619995161, Iran.

devices. Squires and Bazant [5] described the general phenomenon of induced-charge electro-osmosis (ICEO) which includes a wide variety of techniques for driving steady micro-flows around conducting or dielectric surfaces using different electric fields. Arulanandam and Li [6] studied the fluid movement in a rectangular microtube produced by electroosmosis. To model the problem, two-dimensional potential and momentum equations were used in their research. The flow field and volumetric flow rate were presented as functions of the related electrical and geometrical parameters. Dutta and Beskok [7] presented analytical expressions for the relevant hydrodynamic quantities in mixed electroosmotic/pressure driven flows for 2-D straight channel geometry. They also introduced three new concepts regarding the EDL near walls. Tang et al. [8] presented axisymmetric lattice Boltzmann models to solve the electric potential distribution and the velocity field in axisymmetric microducts. They also examined the effect of non-Newtonian fluids on the flow behavior. Wang and Kang [9] numerically solved the dynamic model of electrokinetic flows in microchannels using coupled lattice Boltzmann methods. Xuan and Li [10] developed general solutions to investigate electroosmotic flows in microchannels with arbitrary cross-sectional geometry and various distribution of wall charge. They found that the wall charge affects EOF much greater than the channel geometry. Kang et al. [11] solved the electroosmotic flow problem in a cylindrical channel for only sinusoidal waveform by the Green's function method. Limiting cases of zero frequency and pulsed electric fields were also examined. Tsao [12] studied the electroosmotic flow through an annulus under the constant electric field condition. The thin and thick EDLs were also analyzed. Kang et al. [13] investigated the steady-state EOF in a capillary annulus under the situation when the two cylindrical walls carry high zeta potentials. In their study, the non-linear term of the Poisson-Boltzmann equation has been approximated by some proposed relations. The EOF characteristics thru the annulus were also discussed.

Erickson and Li [14] investigated AC electroosmotic flow in a rectangular microchannel; they also employed a combined theoretical and numerical approach to examine the effect of important parameters on the flow characteristics. Comprehensive models for a slit channel have also been presented by Dutta and Beskok [15] who developed an analytic model for an applied sinusoidal electric field. The difference of the current problem and the Stokes' second problem was also explained. Green et al. [16] experimentally examined the non-uniform electric field interacting with the suspending fluid; they reported peak flow velocities on the order of hundreds of micrometers per second near a set of parallel electrodes subject to two AC fields, 180 degrees out-of-phase with each other. The effect was subsequently modeled [17] using a linear double layer analysis and a good correlation was then found. Using a similar principal, both Brown et al. [18] and Studer et al. [19] introduced microfluidic devices that incorporated arrays of non-uniformly sized embedded electrodes which, when subject to a time-periodic electric field, were able to generate a bulk fluid flow. Moghadam [20–22] presented analytic solutions of alternating current EOF in various microducts the Green's function method. A variety of the flow fields was obtained utilizing various time-periodic electric currents. Moghadam and Akbarzadeh [23] investigated the behavior of the time-periodic EOF of a non-Newtonian fluid in microchannels using a numerical scheme. They also considered the effect of combined pressure gradient and alternating current electroosmosis on the flow field of a non-Newtonian fluid [24]. Moghadam [25] presented analytic expressions for the two-fluid combined electroosmosis/pressure gradient flow, in which, a conducting liquid is moved by electroosmosis thereby pulling a non-conducting liquid. Transient electroosmotic and pressure-driven flow of two-layer fluids was analytically solved by Su et al. [26] and Gao et al. [27] in slit and rectangular microchannels, respectively. The velocity distributions were also plotted for different involved variables. Using a numerical approach, Moghadam and Akbarzadeh [28] studied the transient characteristics of two-fluid EOF in a microchannel in which both pressure gradient and electroosmis forces were exerted on the non-conducting and conducting fluids, respectively. Stiles et al. [29] proposed a simple method to focus the sample stream by using either a single suction pump or capillary pumping effect. The focused stream width was controlled by varying the relative resistances of the side and inlet channel flows. Parida and Padhy [30] studied EOF of a third-grade fluid inside a microchannel having stretching walls. The continuity, momentum, and linearized Poisson-Boltamann equations were employed to simulate the problem; and then a similarity transformation was introduced to obtain relevant ordinary differential equations. Velocity and friction were calculated and plotted. Paustian et al. [31] investigated an induced-charge alternating current EOF. An array of Janus micropillars was used for breaking the symmetry of the flow; hence the flow was driven by applying AC electric fields. Depending on the slip velocity and micropillar geometry, maximum pressure and flow rate were obtained. Herr et al. [32] conducted analytical and experimental studies of EOF in cylindrical capillaries with non-uniform surface potentials. The results revealed that the dispersion rate in the region supported by EOF increases as the length of EOF-suppressing microcapillary increases. Brask et al. [33] presented theoretical studies on the low-voltage cascade electroosmotic pump using two different approaches. The results were then compared to each other. Dutta et al. [34] reported electroosmotic flow in complex geometries using numerical methods. It was shown that flow control has linear

dependence on the value of the applied electric field. Khan and Dutta [35] analyzed EOF in a cylindrical microchannel for heterogeneous surface charges. They showed that several vortices are formed inside the channel with sinusoidal surface charge distribution. Moghadam [36] recently examined the effects of different excitation waveforms (square and triangular) as well as hydraulic diameter on hydrodynamic behavior of time-periodic EOF in a microannulus; the combined waveforms were also studied in the paper. The equal- and unequal-frequency combined waves result in completely different flow characteristics and hence can be utilized in various practical applications.

One of the motivating factors behind the current research is to achieve a better theoretical insight regarding the hydrodynamic behavior of unsteady EOF in a general category of microtubes. Microchannels that are the basic components of microfluidic systems can have various cross-sectional forms (rectangular, triangular, circular, etc.) depending on the material in which they are embedded. To the author's knowledge, there is a lack of research in determining hydrodynamic properties of fluid flow in general rectangular annulus microchannels under the effects of AC electroosmosis. This paper aims to provide a theoretical analysis for time-periodic electrokinetic flow of a Newtonian liquid in a microannulus with various inner/outer surface charges. The flow depends on the combined effects of the geometrical, potential, and hydrodynamic characteristics. Compared to the previous researches, current study concerns two-dimensional AC EOF in rectangular annuli which are the general form of two limiting cases (slit and rectangular cross-sections). The concept of the effective EDL thickness, the Stokes' penetration depth, and the aspect ratio (a measure of the channel shape, even in the case of fixed hydraulic diameter) are introduced in the current research (with respect to the sinusoidal-unsteady electric field). The effects of hydraulic diameter and other key parameters such as frequency on the potential and flow characteristics are comprehensively discussed too. The fundamental features of the potential and velocity fields are investigated in the general form of the geometry. It is noted that the sine wave can be viewed as a basis for other waveforms (i.e. square, triangular, etc. waves are normally made by sine), and the main results of the present research is therefore comparable to those in [36].

2 Potential and velocity fields

According to Fig. 1, the inner and outer surfaces of a rectangular microannulus are uniformly held at $\zeta_I = \beta\zeta_O$ and ζ_O, respectively. If a sinusoidal electric field is axially applied to the capillary, a time-dependent electroosmotic flow is produced. For the sake of brevity, as the geometry and numerical approach are similar to [36], its basic formulation is only written here.

Following [36], the dimensionless potential distribution equation:

$$\frac{\partial^2 \Psi}{\partial X^2} + \frac{\partial^2 \Psi}{\partial Y^2} = \chi^2 \sinh(\Psi) \tag{1}$$

with respect to the boundary conditions:

$$\begin{aligned} X &= \pm L_{XI}, \quad \Psi = \beta Z_O; \quad Y = \pm L_{YI}, \quad \Psi = \beta Z_O \\ X &= \pm L_{XO}, \quad \Psi = Z_O; \quad Y = \pm L_{YO}, \quad \Psi = Z_O \end{aligned} \tag{2}$$

as well as the dimensionless momentum equation:

$$\frac{\partial V}{\partial \theta} = \frac{\partial^2 V}{\partial X^2} + \frac{\partial^2 V}{\partial Y^2} + \chi^2 \sinh(\Psi) F(\Omega\theta) \tag{3}$$

with respect to $V = 0$ on the boundaries are re-written here [36–38]. The electrokinetic diameter χ is equal to κD_h in which, κ is the Debye-Hückel parameter and $D_h = 4A_{c-s}/P_w$ is the channel hydraulic diameter (A_{c-s} and P_w are the cross-sectional area and the wetted perimeter of the channel, respectively). Under the Debye-Hückel approximation together with the selection of $F(\Omega\theta) = \sin(\Omega\theta)$, the above potential and velocity equations are numerically solved [36, 39] using a finite difference approach with a non-uniform rectangular grid (Fig. 2).

Afterwards Poiseuille number and volumetric flow rate are easily calculated in the domain by the following relations:

$$Po = \begin{cases} 2\left|\frac{\partial V}{\partial X}\right|_{L_{XI},L_{XO}} \\ 2\left|\frac{\partial V}{\partial Y}\right|_{L_{YI},L_{YO}} \end{cases} \quad Q = \int_{A_c} V dA \approx \sum_{i,j} V_{i,j}(\Delta A)_{i,j} \tag{4}$$

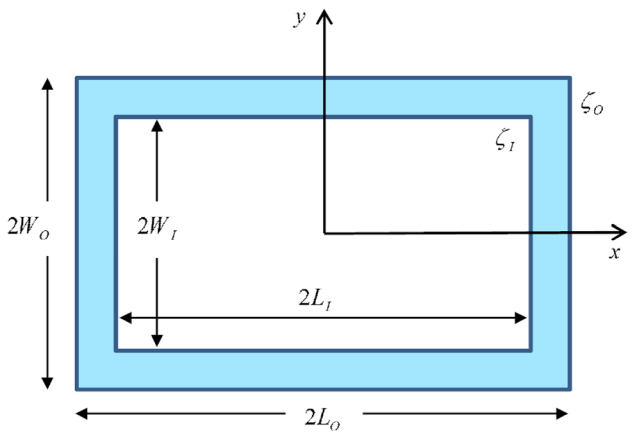

Fig. 1 The geometry of the flow field

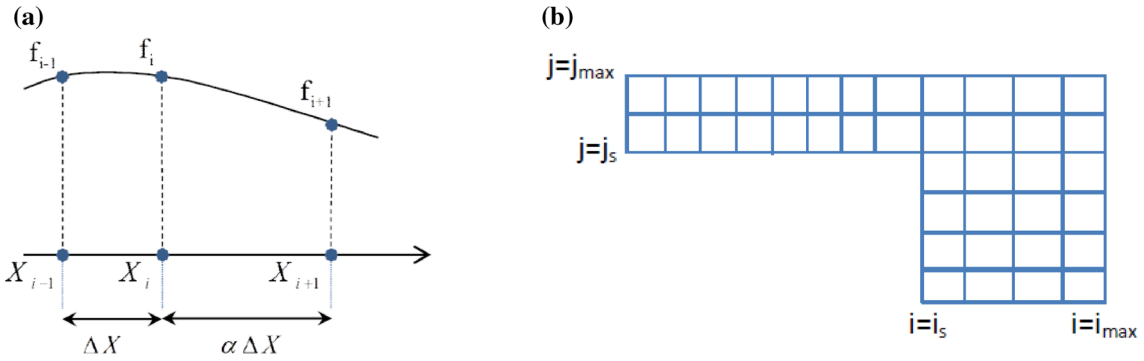

Fig. 2 **a** Central difference with non-uniform mesh, **b** one-fourth of the flow field

3 Results

A parametric study was performed to investigate the effects of governing parameters on the hydrodynamic characteristics of electroosmotic flow in a micro-capillary under the influence of the applied sinusoidal wave form. The non-dimensional zeta potential of the outer wall, $Z_0 = 0.5$, corresponds to $\zeta_0 = 12.5 \times 10^{-3}$ V which is inside the range of the Debye-Hückel approximation. The sign of β determines the relative direction of fluid particles near the inner and outer walls (depending on the requirement). The non-dimensional geometrical dimensions were normally chosen so as to get $D_h = 1$ μm in most cases; another value of the hydraulic diameter, $D_h \cong 1.2154$ μm, is also examined. Another geometrical quantity named aspect ratio (A.R.) is also introduced which is the ratio of the relative width to the height of the microchannel $\left(\text{A.R.} = L_{IO}/W_{IO}\right)$. It is noted that $L_{IO} = L_I/L_O$ and $W_{IO} = W_I/W_O$. Two different values of the aspect ratio have been studied with the constancy of the hydraulic diameter $\left(D_h = 1\ \mu\text{m}\right)$: A.R. $\cong 2.083$ with $L_{IO} = 0.625$, $W_{IO} = 0.3$ and A.R. $\cong 0.533$ with $L_{IO} = 0.4$, $W_{IO} = 0.75$. A broad range of non-dimensional frequency, $0.3 \le \Omega \le 3000$, has been selected to deal with the essential aspects of the flow field. Due to the symmetry, only one-fourth of the cross-sectional area is considered here.

Figure 3a, b shows typical dimensionless potential distributions at the X-symmetry plane $\left(\text{for } D_h = 1\ \mu\text{m},\ \text{A.R.} = 1\right)$. The potential field falls sharply to zero; hence there is a small region close to the channel surface where the net charge density is non-zero. As χ is increased, the non-zero potential area will be thinner (Fig. 3a).

Our analysis is generally valid for the cases where the EDL thickness is smaller than the channel hydraulic diameter; hence, the electroosmotic potential distributions from the walls do not interact with each other. This condition is expressed by the *effective EDL thickness*, $\delta_{1\%N}$, which is defined as the distance from the channel wall where the dimensionless electroosmotic potential reaches 1% of its base value [15]. For $Z_0 = 0.5$, as shown in Fig. 3b, $\delta_{1\%N}\big|_{\text{outer}} \cong 0.0105$ is achieved when Ψ reaches 0.005. As $\chi = \kappa D_h$ and $\lambda_D = 1/\kappa$ are the electrokinetic diameter and the debye length, respectively, for $D_h = 1$ μm and $\chi = 1000$, we obtain $\delta_{1\%}\big|_{\text{outer}} = 1.05 \times 10^{-8}$ m and $\lambda_D = 10^{-9}$ m and therefore, $\delta_{1\%}\big|_{\text{outer}} = 10.5\lambda_D$. Figure 3c, d represent the near-outer wall velocity profiles with their effective EDL thicknesses for two Ω values. The velocity increases rapidly from zero (on the wall) to its extremum within the EDL region where the electrical forces exist. The fluid outside this active area moves due to the frictional stresses originating from liquid viscosity.

Table 1 shows variations of the effective EDL thickness with χ and D_h. It indicates that a rise in χ leads to a fall in $\delta_{1\%}$; while the influential ratio $\delta_{1\%}/\lambda_D$ increases due to the reduced Debye length. The last two rows of Table 1 typically show that, by comparison, the slit and rectangular microchannels have the larger and smaller values of $\delta_{1\%}/\lambda_D$, respectively.

The velocity fields for different values of Ω are compared in Fig. 4 in which the left and right columns are for $\Omega = 0.3$ and $\Omega = 30$, respectively $\left(\text{for } D_h = 1\ \mu\text{m},\ \text{A.R.} = 1\right)$. Dimensionless frequency can be viewed as the hydraulic diameter of the microchannel to the Stokes' penetration depth $\Omega = \left(D_h/\delta_S\right)^2$ in which, $\delta_S = \sqrt{\nu/\omega}$ [15]. Hence, in the case of $D_h = 1$ μm for instance, δ_S will be 1.826 μm and 0.0182 μm for $\Omega = 0.3$ and $\Omega = 3000$, respectively. The lower the frequency, the more the penetration depth will be. It is also the ratio of the time scale for viscous diffusion to the period of oscillation. When $\Omega < 1$, momentum diffusion is faster than the period of oscillation and thus, the bulk liquid reacts immediately to instantaneous changes in the applied electric field, and a plug flow (a flow cell) with a nearly constant velocity is achieved across the channel over a period of time. When $\Omega > 1$, however, an out of phase behavior is observed in the bulk liquid; that is, despite the fluid within the EDL, the response of the bulk

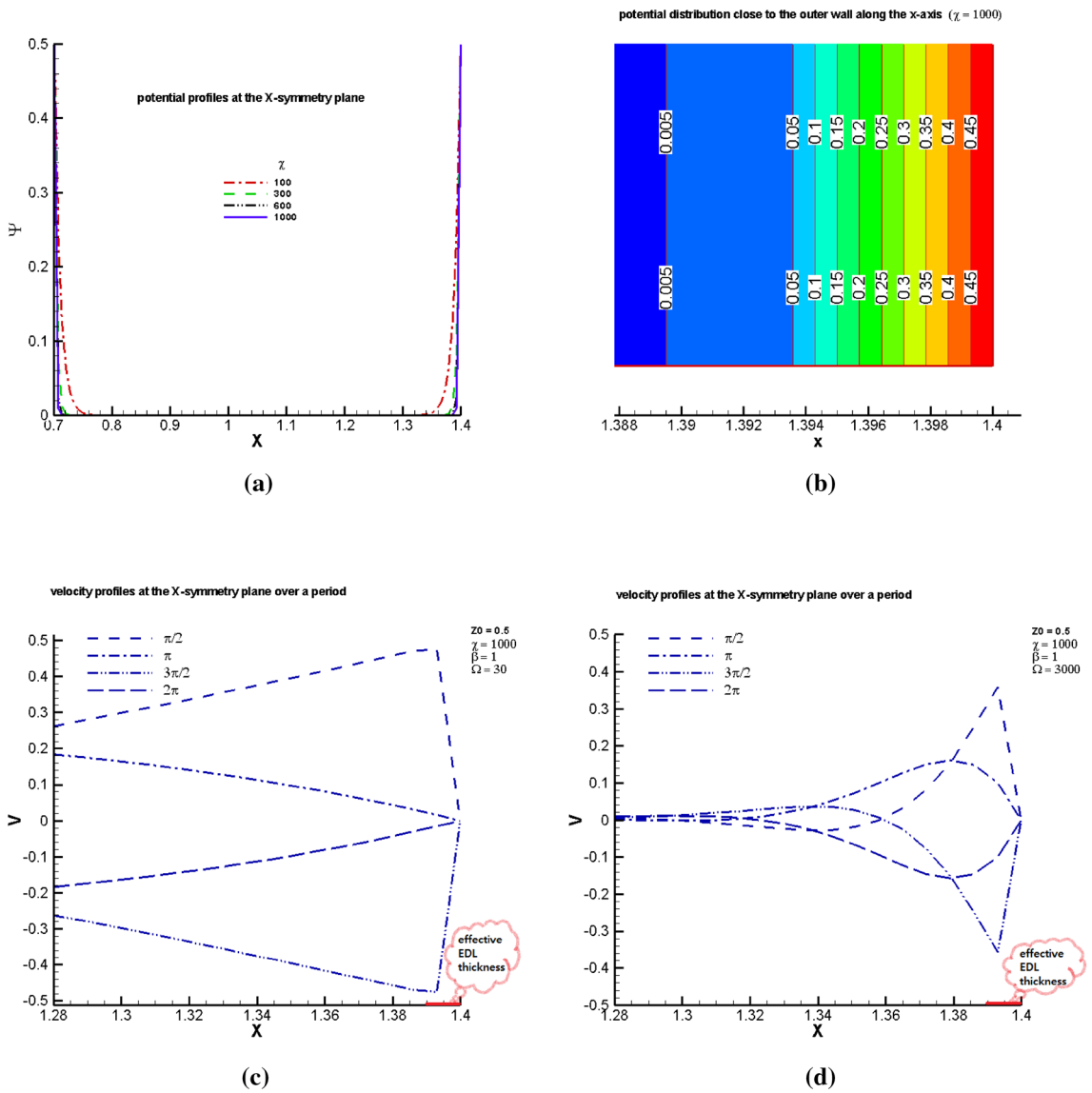

Fig. 3 **a** Profiles of Ψ at the X-symmetry plane for $Z_0 = 0.5$ and four χ values, **b** distribution of Ψ near the outer wall; **c**, **d** profiles of V at the X-symmetry plane near the outer wall for two Ω values

Table 1 Variations of $\delta_{1\%}$ with χ and D_h

D_h (μm)	χ	$\delta_{1\%N}$	$\delta_{1\%}$ (nm)	λ_D(nm)	$\frac{\delta_{1\%}}{\lambda_D}$
1	100	0.0475	47.5	10	4.75
1	300	0.019	19	10/3	5.7
1	600	0.013	13	5/3	7.8
1	1000	0.0105	10.5	1	10.5
0.9294118	1000	0.0103	9.573	0.9294118	10.3
1.215385	1000	0.0099	12.03	1.215385	9.9
0.2	1000	0.0225	4.5	0.2	22.5
1.8	1000	0.00738	13.284	1.8	7.38

fluid to the time-dependent electric field will have a finite time delay.

These occurrences can further be realized by an illustration of velocity evolution of some representative points with time (Fig. 5). The labels 1, 2, and 3 indicate the points located at the inner-wall EDL, in the middle of the channel, and at the outer-wall EDL, respectively, along the X-symmetry plane. The applied sinusoidal electric field is designated by sine.

Apparently when $\Omega < 1$, all points follow the applied electric field without any considerable time delay. If $\Omega > 1$, however, the delays are significantly different in the double layers (points 1 and 3) than in the bulk liquid (point 2); also, the velocity magnitude of point 2 will relatively be

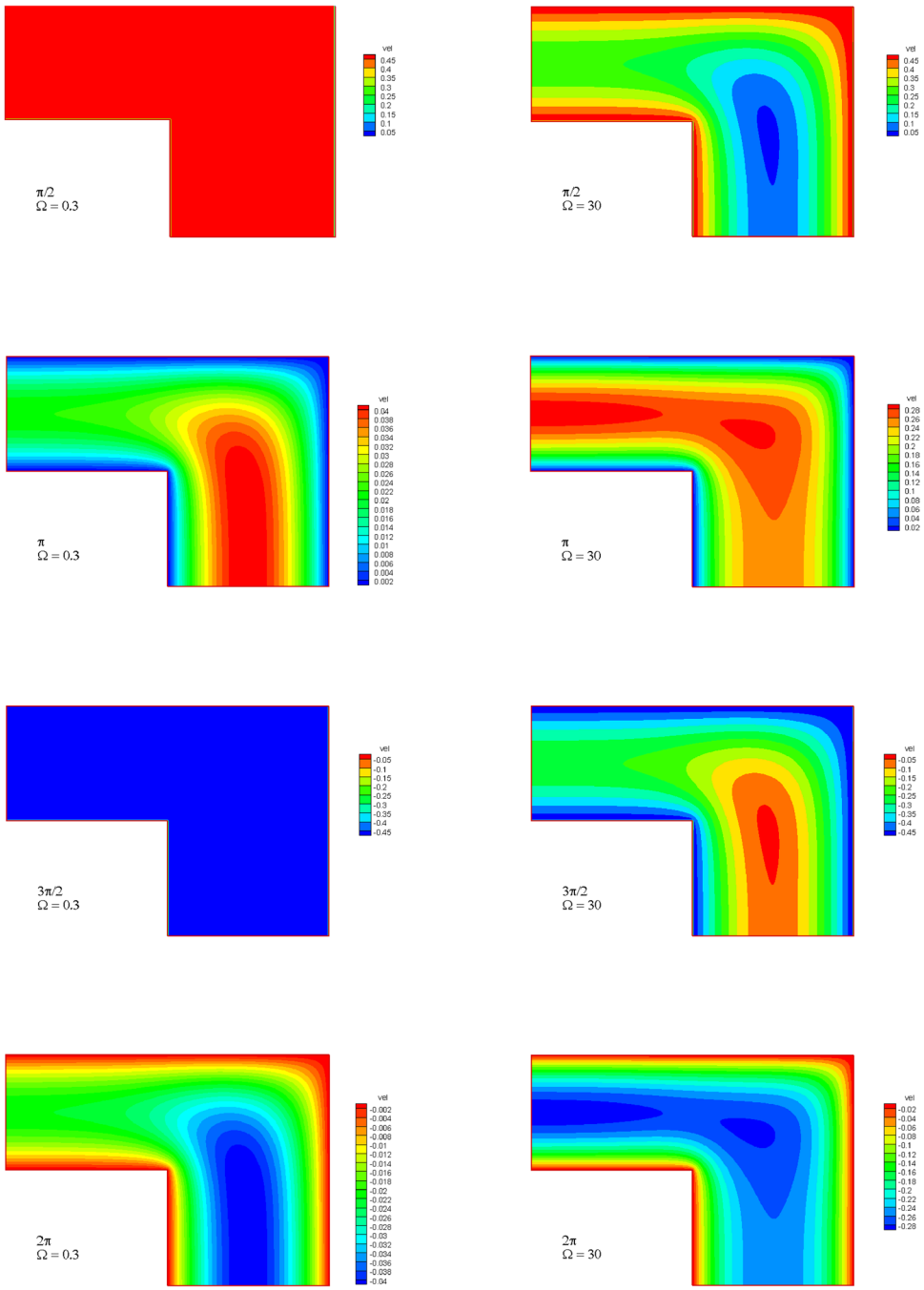

Fig. 4 Velocity contours over a period of time for $Z_O = 0.5$, $\chi = 1000$, $\beta = 1$, and two various Ω

smaller than that of points 1 and 3. The higher the dimensionless frequency, the more time delay (phase shift) occurs in the bulk fluid. Meanwhile, for moderate to high-frequency values, the fluid within the double layer reaches its quasi-steady-state oscillation almost immediately, but the rest requires a period-of-time before the transient effects diminish. For very high dimensionless frequencies (e.g. $\Omega = 3000$), the velocity in the channel mid-point is practically zero (Fig. 5d).

Figure 6 shows velocity profiles at the X- and Y-symmetry planes for various values of Ω (for $D_h = 1$, A.R. $= 1$). As remarked above, a lid-like velocity profile is attained for $\Omega = 0.3$. On the contrary, when Ω is very large ($\Omega = 3000$), the near-wall liquid oscillates rapidly while the bulk fluid remains immobile; since there is not sufficient time for momentum to diffuse further into the remaining part of the fluid. These behaviors and trends are in agreement with the results of [35], e.g. with Fig. 4, in which, the velocity contours were plotted for small and large frequencies. As can be seen, the central portion of the channel is stationary for very large values of the frequency. On the contrary, when the frequency

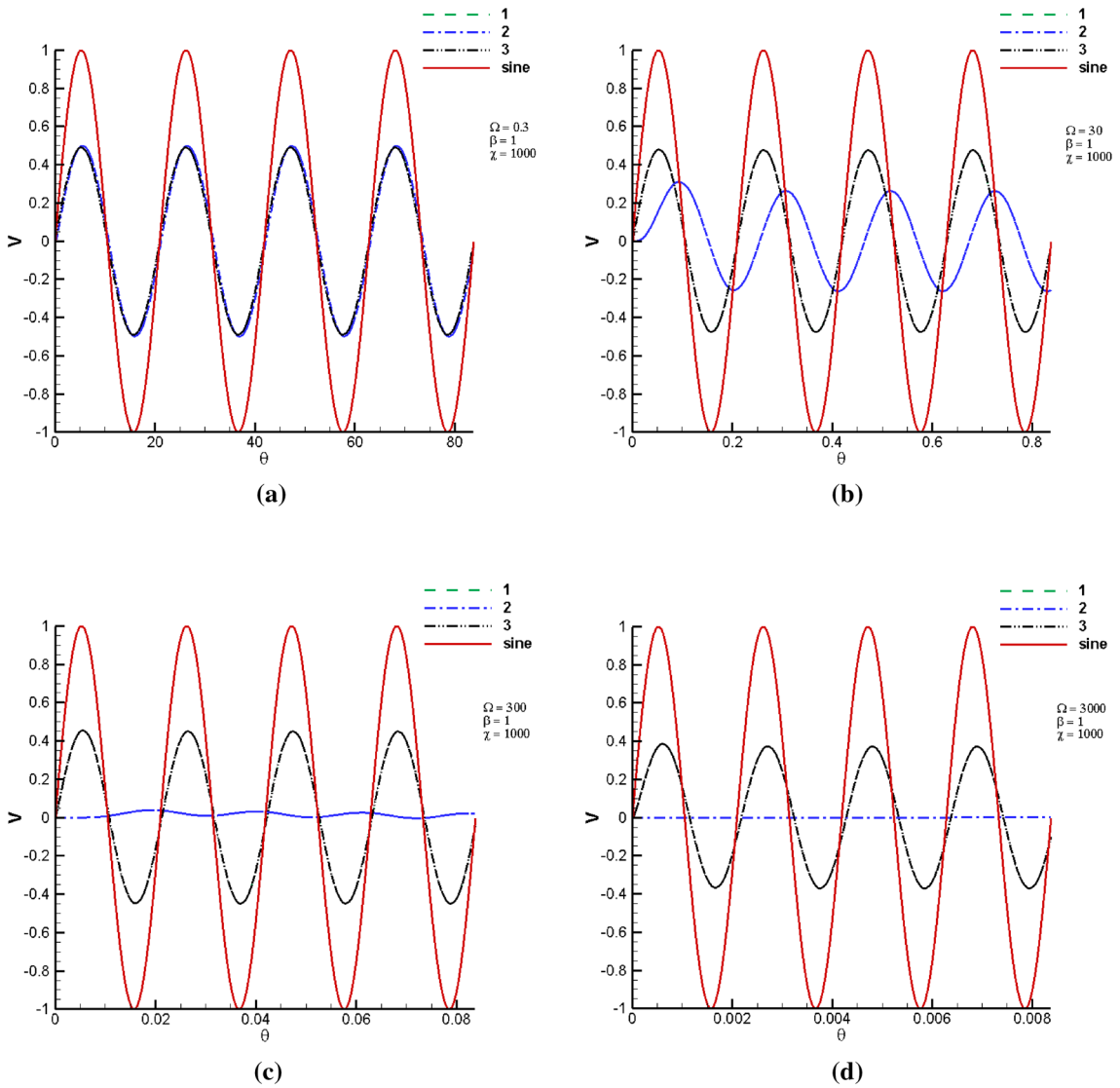

Fig. 5 Transient and quasi-steady-state velocity magnitudes of some typical points

becomes sufficiently small, non-zero-velocity cells are observed in the middle of the channel section. For moderate amounts of the dimensionless frequency (i.e., $\Omega = 30$), however, the bulk fluid can follow the sinusoidal electric field with a time delay. The EDL field is impacted by the channel geometry too. The gap sizes (the distance between the walls) in the X- and Y-symmetry planes are 0.7 and 0.5, respectively.

A comparison of the left and right columns (in one row) reveals that the larger area of the flow field is affected if the gap size is smaller; because as the gap size decreases, the EDL thickness becomes relatively larger and hence the EDL affects stronger.

When the charges of the inner and outer walls are different in sign, as illustrated in Fig. 7 $\left(\text{for } D_h = 1\ \mu\text{m, A.R.} = 1\right)$, the fluid moves in two opposite directions (depending on the polarity of each surface).

In this case (the negative surface charge ratio), there is a thin surface in the cross-sectional area where the velocity magnitude is nearly zero over a period of time. The thickness of this surface (shell) generally varies depending on the gap size around the channel cross-section (also is deducible from Fig. 7c, d).

Effects of χ, Ω and D_h on Q are shown in Fig. 8 for $Z_0 = 0.5$ and $\beta = 1$. Increasing χ by ten times results in increasing Q by three percent at most. An increase in Ω leads to a decrease in Q; this is also entirely consistent with velocity distributions, Figs. 4, 5 and 6 for instance, because a rise in Ω causes the bulk fluid moves slowly

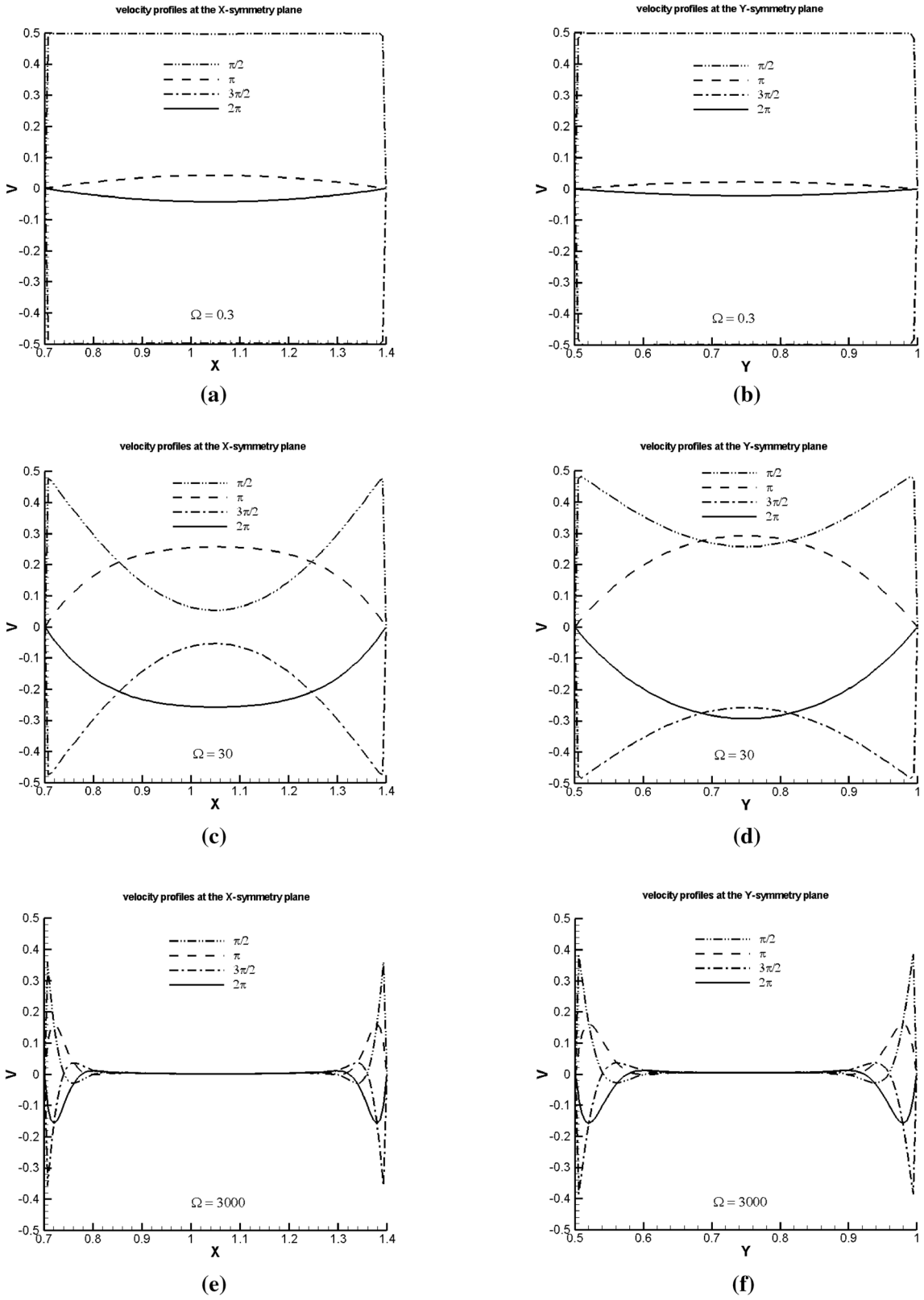

Fig. 6 Velocity profiles for $Z_0 = 0.5$, $\chi = 1000$, $\beta = 1$ at the symmetry planes

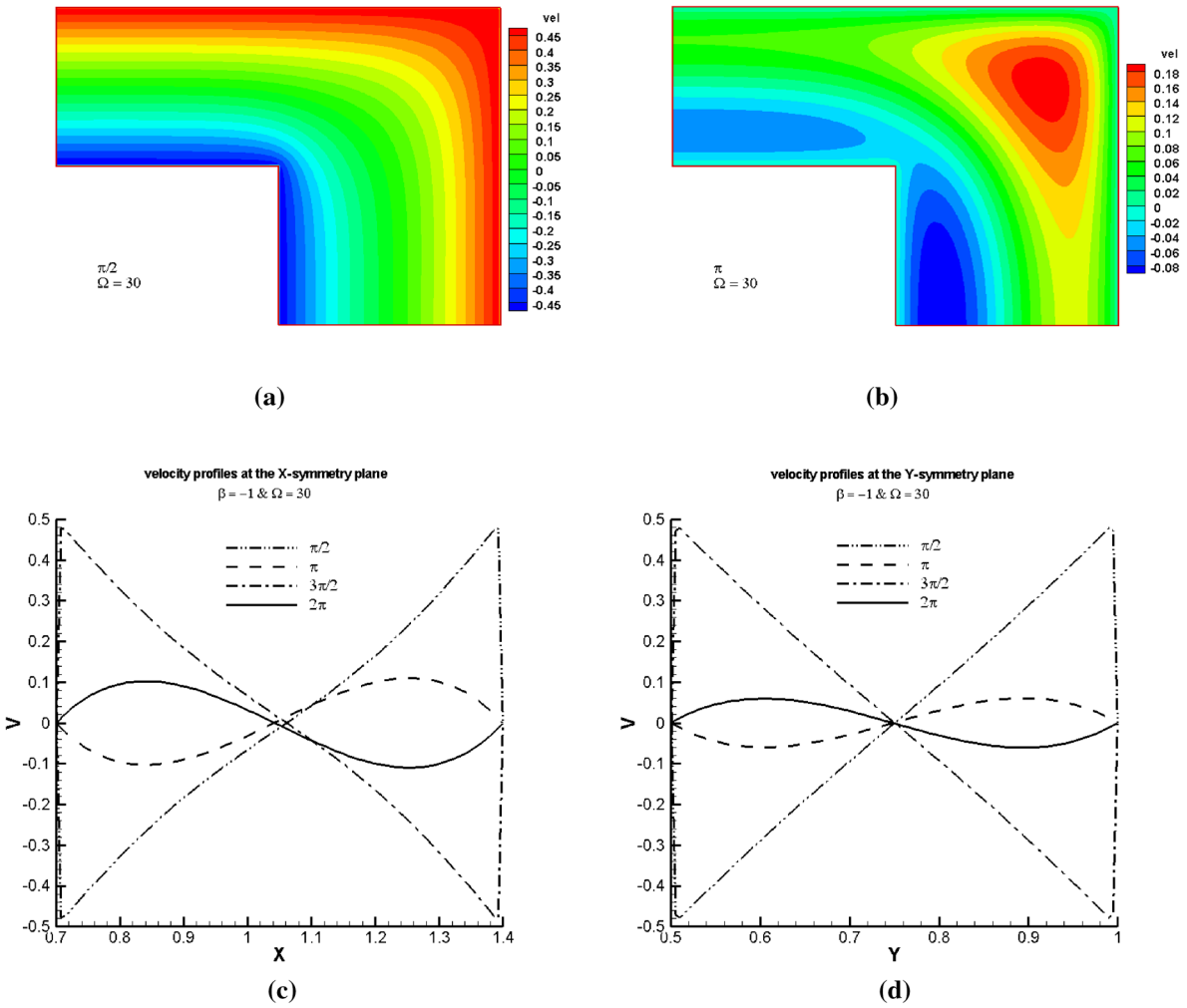

Fig. 7 Velocity distribution for $Z_0 = 0.5$, $\chi = 1000$, and $\beta = -1$; **a**, **b** over a half period, **c**, **d** at the symmetry planes over a period of time

relative to the fluid inside the EDL and so a significant reduction in the flow rate occurs. For fixed values of χ and Z_0, as seen in Fig. 8b, c, Q is approximately in inverse proportion to $(D_h)^2$. This can be explained, on the one hand, by the constancy of the electrokinetic diameter, and on the other hand, by reducing the influential ratio $(\delta_{1\%}/\lambda_D)$; in fact, the influence of the EDL on the bulk fluid will comparatively be weakened. Moreover, the ratio of A_{c-s}/P_w increases with D_h; the relative perimeter of the channel decreases, hence a reduction in the ratio of the electric to viscous forces happens.

Poiseuille number is studied in Fig. 9 for various values of χ, Ω, and β over transient and quasi-steady-state periods of time. As Po is directly related to the velocity gradient at the wall, it has obviously an oscillatory behavior. By decreasing χ, for a fixed hydraulic diameter, the Debye length is increased and therefore lower velocity gradient is attained close to the wall. The Po_m values of 83.42, 79.57, 67.76, and 37.5 are calculated for the χ values of 1000, 600, 300, and 100, respectively. Similar trend is observed for increasing Ω.

The Po_m values of 83.07, 83.42, 82.52, and 78.89 are calculated for the Ω values of 0.3, 30, 300, and 3000, respectively. When $\Omega = 3000$, as a result of the initial impulse given to the system, Po demonstrates higher magnitudes in the transient period before decaying into the quasi-steady-state behavior. If the inner wall zeta potential is negative ($\beta = -1$in Fig. 9c), the same result of Fig. 9a for $\chi = 1000$ will be obtained because Po depends on the absolute value of the wall velocity gradient. As remarked above, Fig. 9d also shows that Po_m decreases with Ω. A rise in D_h, for a fixed χ, leads to a rise in Po_m; since the ratio of the electric body force to the viscous retardation force is reduced.

It is noteworthy that, to perform appropriate comparisons, the horizontal axis of Figs. 8b, c, and 9b have been scaled down for dimensionless frequencies smaller than 3000; in fact, θ must be extended 10, 100, and 10000 times

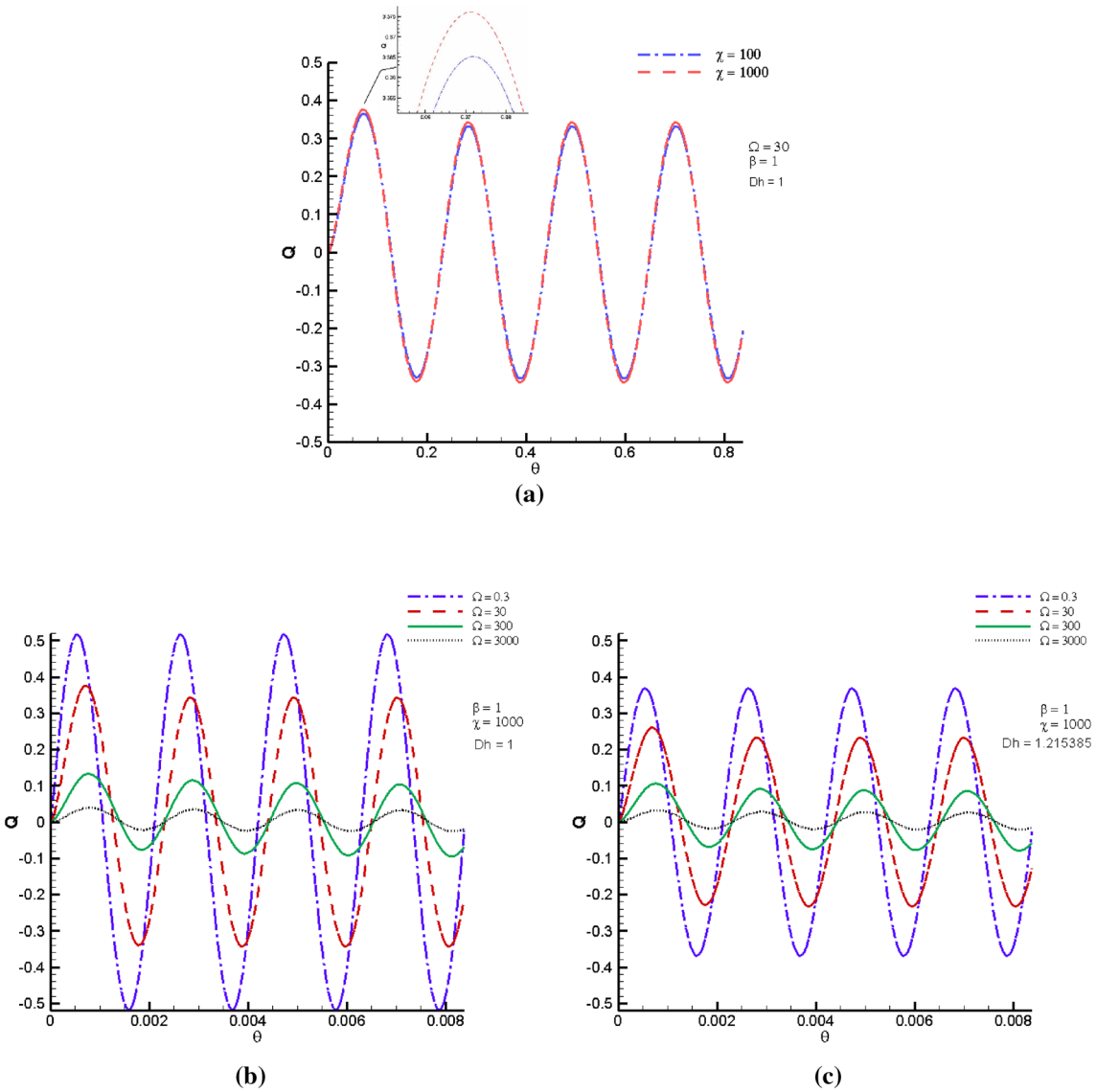

Fig. 8 Volumetric flow rate over the first four periods for $Z_0 = 0.5$, $\beta = 1$; **a** effect of χ, **b**, **c** effect of Ω for two different values of D_h

longer for the Ω values of 300, 30, and 0.3, respectively. Meanwhile $D_h = 1$ μm and A.R. = 1are set for Figs. 8 and 9 (obviously, except 8c and 9d).

Figure 10a, b illustrates Q for two various values of A.R. that is also comparable to that in Fig. 8b (with A.R. = 1). With a rectangular microannulus, not only D_h but also the aspect ratio (in fact, the channel shape) may influence the hydrodynamic characteristics thru the impact of the channel geometry on the EDLs. As depicted in the figures, increasing A.R. (for a fixed hydraulic diameter) results in an increase in Q and vice versa. As the aspect ratio approaches 1and even smaller (e.g.0.533), the flow rate decreases; this can be eventually owing to the larger role that edge and corner effects have on the development of the EDL and the velocity profile in non-circular cross-sections.

Figure 10c, d together with 9b compare the relationship between *Po* and A.R. in which a fall in the aspect ratio leads to a big rise in the Poiseuille number that is in agreement with the corresponding trend of the flow rate. For $D_h = 1$ μm and A.R. ≅ 0.533, for instance, the average Poiseuille number values of 116.8 and 113.09 are obtained for $\Omega = 0.3$ and $\Omega = 3000$, respectively, which is comparable with the corresponding values of 83.07 and 78.89 for A.R. = 1.

4 Conclusions

In this research, the time-periodic EOF of a Newtonian liquid is analyzed in a rectangular microannulus. The impact of the basic sinusoidal waveform as well as the geometrical

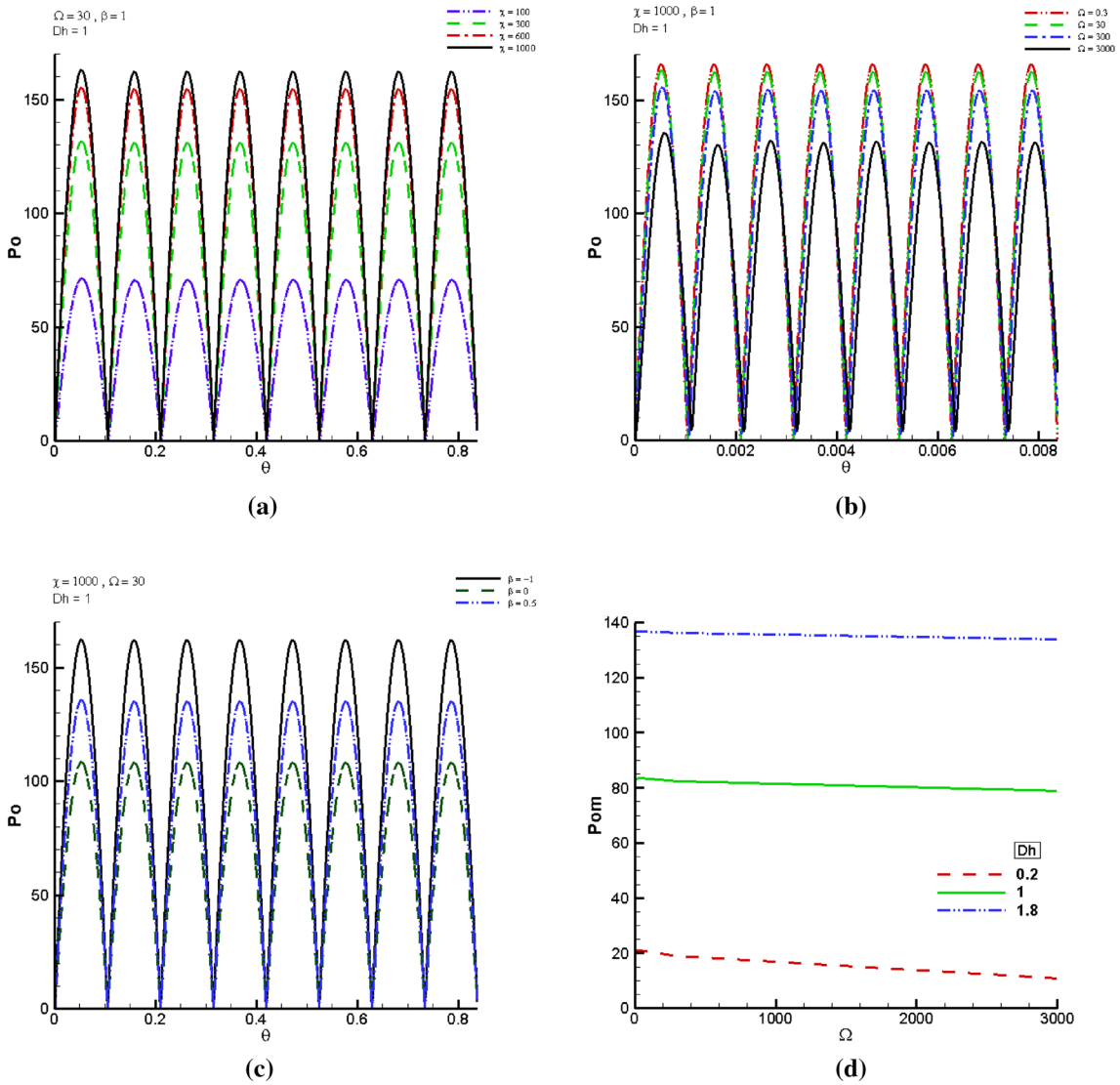

Fig. 9 Variations of *Po* with **a** χ, **b** Ω, and **c** β; **d** Po_m versus Ω for three different values of D_h

considerations on the flow behavior is completely discussed. The outcomes of the current study are summarized below:

1. The shape of the microchannel (primarily thru the hydraulic diameter and the aspect ratio) affects the potential and velocity distributions. A decrease in the gap size leads to a relatively larger EDL thickness; as a result, the flow field broadens. The effective EDL thickness decreases with increasing the electrokinetic diameter. With the constancy of the hydraulic diameter, a rise in the aspect ratio may result in a rise in the flow rate (while a fall in the Poiseuille number).
2. When dimensionless frequency is smaller than unity, complete flow cells are observed at nearly all times. When dimensionless frequency is greater than unity, the fluid within the EDL exhibits an immediate response to the instantaneous changes in the applied electric field; however, the bulk fluid has a time delay depending on the frequency magnitude.
3. In the case of very high dimensionless frequency (i.e., high excitation frequency, large annulus size or small kinematic viscosity), the flow is mainly restricted to a region close to the channel walls while the rest of the flow field remains almost stationary.
4. In the case of oppositely-charged walls, the two-direction flow field is observed where a thin shell exists whose velocity is almost zero over a period of time.
5. An increase in the dimensionless frequency and/or in the hydraulic diameter, with the constancy of the electrokinetic diameter, may result in decreasing the flow rate.

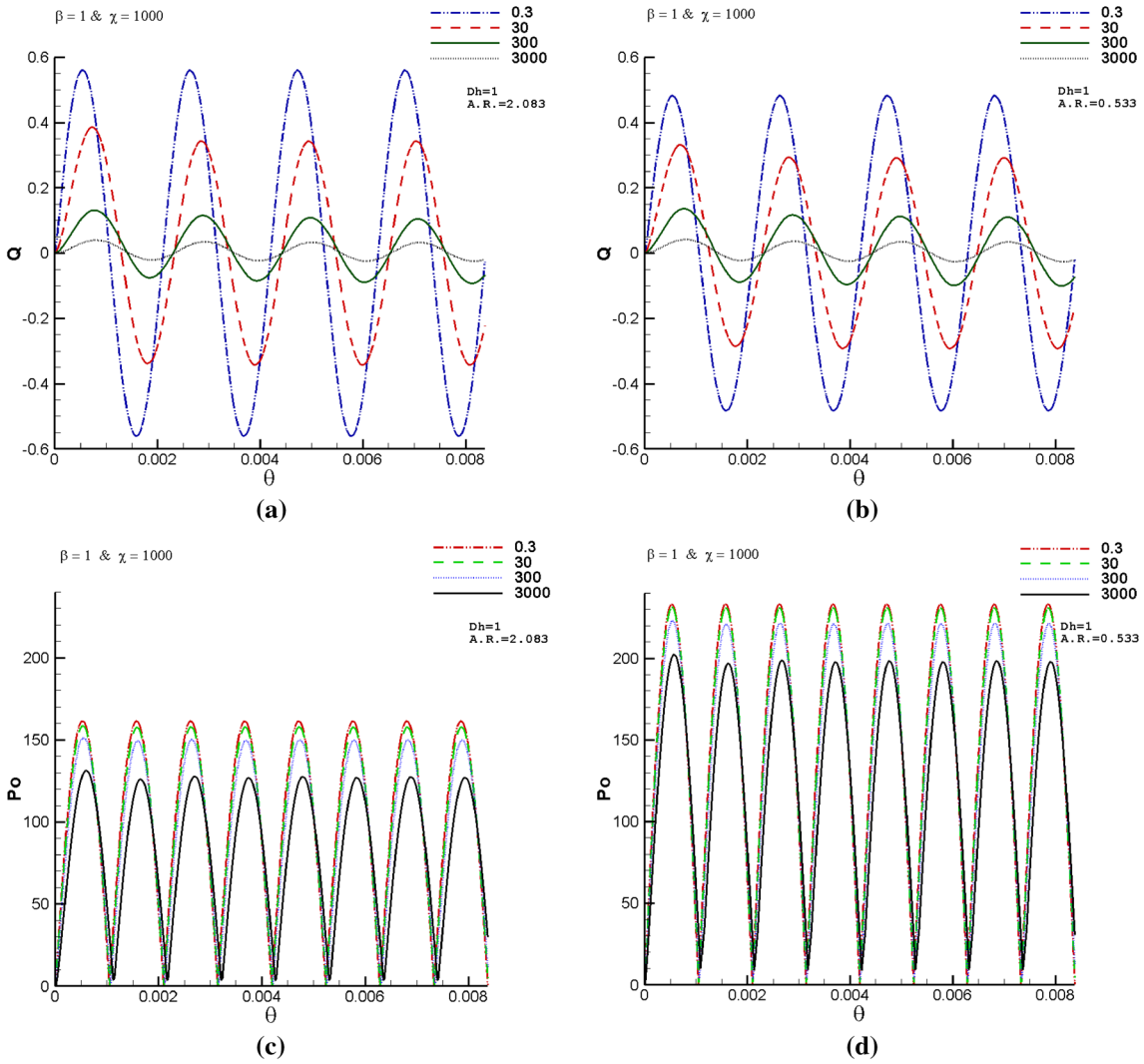

Fig. 10 Effects of A.R. on *Q* and *Po* for four different *Ω* values

6. Poiseuille number and flow rate increase by increasing the electrokinetic diameter and/or decreasing dimensionless frequency. An increase in the hydraulic diameter leads to an increase in the Poiseuille number (for a fixed electrokinetic diameter).

Compliance with ethical standards

Conflict of interest The author states that there is no conflict of interest.

References

1. Bruus H (2008) Theoretical microfluidics. Oxford University Press, Oxford
2. Nguyen NT, Wereley ST (2006) Fundamentals and applications of microfluidics. Artech House, Norwood
3. Tabeling P (2005) Introduction to microfluidics. Oxford University Press, Oxford
4. Li D (2004) Electrokinetics in microfluidics. Elsevier Academic Press, Amsterdam
5. Squires TM, Bazant MZ (2004) Induced-charge electro-osmosis. J Fluid Mech 509:217–252

6. Arulanandam S, Li D (2000) Liquid transport in rectangular microchannels by electro-osmotic pumping. Colloids Surf A 161:89–102
7. Dutta P, Beskok A (2001) Analytical solution of combined electroosmotic/pressure driven flows in two-dimensional straight channels: finite Debye layer effects. Anal Chem 73:1979–1986
8. Tang GH, Li XF, Tao WQ (2010) Microannular electro-osmotic flow with the axisymmetric lattice Boltzmann method. J Appl Phys 108:114903
9. Wang M, Kang Q (2010) Modeling elctrokinetic flows in microchannels using coupled lattice Boltzmann methods. J Comput Phys 229:728–744
10. Xuan XC, Li D (2005) Electroosmotic flow in microchannels with arbitrary geometry and arbitrary distribution of wall charge. J Colloid Interface Sci 289:291–303
11. Kang YJ, Yang C, Huang XY (2002) Dynamic aspects of electroosmotic flow in a cylindrical microcapillary. Int J Eng Sci 40:2203–2221
12. Tsao HK (2000) Electroosmotic flow through an annulus. J Colloid Interface Sci 225:247–250
13. Kang YJ, Yang C, Huang XY (2002) Electroosmotic flow in a capillary annulus with high zeta potentials. J Colloid Interface Sci 253:285–294
14. Erickson D, Li D (2003) Analysis of alternating current electroosmotic flows in a rectangular microchannel. Langmuir 19:5421–5430
15. Dutta P, Beskok A (2001) Analytical solution of time periodic electroosmotic flows: analogies to stokes second problem. Anal Chem 73:5097–5102
16. Green NG, Ramos A, Gonzalez A, Morgan H, Castellanos A (2000) Fluid flow induced by non-uniform AC electric fields in electrolytes on microelectrodes I: experimental measurements. Phys Rev E 61:4011–4018
17. Gonzalez A, Ramos A, Green NG, Castellanos A, Morgan H (2000) Fluid flow induced by non-uniform AC electric fields in electrolytes on microelectrodes II: a linear double layer analysis. Phys Rev E 61:4019–4028
18. Brown ABD, Smith CG, Rennie AR (2002) Pumping of water with an AC electric field applied to asymmetric pairs of microelectrodes. Phys Rev E 63:016305
19. Studer V, Pepin A, Chen Y, Ajdari A (2002) Fabrication of microfluidic devices for AC electrokinetic fluid pumping. Microelectron Eng 61–62:915–920
20. Moghadam AJ (2012) An exact solution of AC electro-kinetic-driven flow in a circular micro-channel. Eur J Mech B Fluids 34:91–96
21. Moghadam AJ (2013) Exact solution of AC electro-osmotic flow in a microannulus. ASME J Fluids Eng 135:091201
22. Moghadam AJ (2014) Effect of periodic excitation on alternating current electroosmotic flow in a microannular channel. Eur J Mech B Fluids 48:1–12
23. Moghadam AJ, Akbarzadeh P (2016) Time-periodic electroosmotic flow of non-Newtonian fluids in microchannels. Int J Eng Trans B 29:736–744
24. Moghadam AJ, Akbarzadeh P (2017) Non-Newtonian fluid flow induced by pressure gradient and time-periodic electroosmosis in a microtube. J Braz Soc Mech Sci Eng 39:5015–5025
25. Moghadam AJ (2016) Two-fluid electrokinetic flow in a circular microchannel. Int J Eng Trans A 29(10):1469–1477
26. Su J, Jian YJ, Chang L, Liu QS (2013) Transient electro-osmotic and pressure driven flows of two-layer fluids through a slit microchannel. Acta Mech Sin 29:534–542
27. Gao Y, Wong TN, Yang C, Ooi KT (2005) Transient two-liquid electroosmotic flow with electric charges at the interface. Colloids Surf A 266:117–128
28. Moghadam AJ, Akbarzadeh P (2019) AC two-immiscible-fluid EOF in a microcapillary. J Braz Soc Mech Sci Eng 41:194. https://doi.org/10.1007/s40430-019-1702-2
29. Stiles T, Fallon R, Vestad T, Oakey J (2005) Hydrodynamic focusing for vacuum-pumped microfluidics. Microfluid Nanofluid 1:280–283
30. Parida M, Padhy S (2019) Electro-osmotic flow of a third-grade fluid past a channel having stretching walls. Nonlinear Eng 8(1):56–64
31. Paustian JS, Pascall AJ, Wilson NM, Squires TM (2014) Induced charge electroosmosis micropumps using arrays of janus micropillars. Lab Chip 14:3300
32. Herr AE, Molho JI, Santiago JG, Mungal MG, Kenny TW (2000) Electroosmotic capillary flow with nonuniform zeta potential. Anal Chem 72:1053–1057
33. Brask A, Goranovic G, Bruus H (2003) Theoretical analysis of the low-voltage cascade electro-osmotic pump. Sens Actuators B 92:127–132
34. Dutta P, Beskok A, Warburton TC (2002) Electroosmotic flow control in complex microgeometries. J Microelectromech S 11(1):36–44
35. Khan AI, Dutta P (2019) Analytical solution of time-periodic electroosmotic flow through cylindrical microchannel with non-uniform surface potential. Micromachines 10:498. https://doi.org/10.3390/mi10080498
36. Moghadam AJ (2019) Unsteady electrokinetic flow in a microcapillary: effects of periodic excitation and geometry. ASME J Fluids Eng 141:111104
37. Kirby BJ (2010) Micro- and nanoscale fluid mechanics. Cambridge University Press, Cambridge
38. Kandlikar S, Garimella S, Li D, Colin S, King MR (2006) Heat transfer and fluid flow in minichannels and microchannels. Elsevier, Amsterdam
39. Hoffman JD (2001) Numerical methods for engineers and scientists. Marcel Dekker Inc, New York